photonics

Review

Space–Time Duality in Optics: Its Origin and Applications

Govind P. Agrawal

The Institute of Optics, University of Rochester, Rochester, NY 14627, USA; govind.agrawal@rochester.edu

Abstract: The concept of space–time duality in optics was originally based on the mathematical connection between the diffraction of beams in space and the dispersion of pulses in time. This concept has been extended in recent years from the temporal analog of reflection for optical pulses to photonic time crystals in a medium where refractive index varies with time in a periodic fashion. In this review, I discuss how the concept of space–time duality and the use of nonlinear optics has led to many advances in recent years. Starting from the historical origin of space–time duality, time lenses and their applications are reviewed first. Later sections cover phenomena such as soliton-induced temporal reflection, time-domain waveguiding, and the formation of spatiotemporal Bragg gratings.

Keywords: space–time duality; solitons; temporal reflection; nonlinear optics

check for updates

Received: 14 May 2025
Revised: 10 June 2025
Accepted: 11 June 2025
Published: 13 June 2025

Citation: Agrawal, G.P. Space–Time Duality in Optics: Its Origin and Applications. *Photonics* **2025**, *12*, 611. https://doi.org/10.3390/photonics12060611

1. Introduction

In the context of optics, space–time duality was noticed first by Tournois in 1964 [1] and a few years later by Akhmanov et al. [2]. It is based on the mathematical equivalence, under some conditions, of two equations governing the diffraction of beams in space and the dispersion of pulses in time. However, it was only after 1988 that space–time duality was used to develop the concept of a time lens and such lenses were used for temporal imaging [3–5]. As the name suggests, a time lens plays the role of a conventional lens in the time domain and can be used for making the analog of a microscope for imaging a time-varying signal. For this reason, devices acting as time lenses have attracted considerable attention for optical signal processing [6–9].

In recent years, the concept of space–time duality has been extended in several directions. An example in nonlinear optics is provided by the spatial and temporal solitons. The underlying equation describing them is the nonlinear Schrödinger (NLS) equation [10]. Spatial and temporal solitons form when this equation includes the diffractive or dispersive effects, respectively, [11]. In the context of the Kerr frequency combs, adoption of the Lugiato–Lefever equation that was developed originally for spatial cavity solitons led to the observation of temporal cavity solitons [12].

The temporal analog of the phenomenon of reflection, which occurs at any spatial interface separating two media of different refractive indices, constitutes another example of space–time duality [13–15]. In this analog, a temporal interface separates two intervals of different refractive indices in the same medium. It turns out that a moving temporal interface, which changes the refractive index of a dispersive medium in a region moving at a constant speed [16], is easier to realize in practice. When an optical pulse interacts with this moving interface inside a dispersive medium, it splits into two parts, whose frequencies are shifted such that they travel at different speeds [17–20]. These two parts correspond to reflected and transmitted pulses and are temporal analogs of the reflection and refraction at a spatial interface [15]. It is also possible to realize the temporal analog of total internal reflection and to use it for time-domain waveguiding [17].

Wave propagation in a medium whose refractive index varies spatially has a long history. Such an inhomogeneous medium is useful in different contexts such as graded-index fibers [21], Bragg gratings [22], and photonic crystals [23]. Recent attention to time-varying media [24–26], where the refractive index varies with time, constitutes another example of space–time duality. It has led to novel concepts such as photonic time crystals [27–29] and spatiotemporal Bragg gratings [30].

In this review, I discuss how the concept of space–time duality and the use of nonlinear optics has led to multiple advances in recent years. Section 2 reviews the historical origin of space–time duality by focusing on the phenomena of spatial diffraction and temporal dispersion. Time lenses and their applications are reviewed in Section 3. The focus of Section 4 is on the temporal analog of reflection and refraction for optical pulses at a moving temporal boundary inside a dispersive medium. The use of nonlinear effects for creating such boundaries is discussed in Section 5. Optical solitons, forming inside an optical fiber through the Kerr effect, are used to discuss the temporal analogs of spatial reflection, waveguides, and Fabry–Perot resonators. Section 6 is devoted to the case of periodic temporal modulations of a medium's refractive index, leading to the formation of spatiotemporal Bragg gratings and photonic time crystals.

2. Origin of Space–Time Duality

Diffraction and dispersion are fundamental concepts in optics [31,32]. Any optical beam spreads in space because of diffraction, and an optical pulse spreads in time because of dispersion [33]. The initial concept of space–time duality was based on the mathematical equivalence of wave-propagation equations governing these two phenomena under specific conditions [1,2]; it has been extended further in recent years.

Consider propagation of electromagnetic waves in a linear dispersive medium. As it is simpler to solve Maxwell's equations in the frequency domain, it is common to employ the Fourier transform of the electric field in the form

$$\tilde{\mathbf{E}}(\mathbf{r},\omega) = \int_{-\infty}^{\infty} \mathbf{E}(\mathbf{r},t)\, e^{i\omega t}\, dt, \tag{1}$$

and solve the resulting Helmholtz equation,

$$\nabla^2 \tilde{\mathbf{E}} + k^2(\omega)\tilde{\mathbf{E}} = 0, \tag{2}$$

where $k(\omega) = n(\omega)\omega/c$, $n(\omega)$ is the refractive index of the medium at the frequency ω and c is the speed of light in vacuum. This equation can be used for continuous-wave (CW) beams or pulsed beams by choosing a suitable range of frequencies.

Let us first consider a CW beam with a narrow spectrum (nearly monochromatic) centered at a specific frequency ω_0. In this case, $k = n(\omega_0)\omega_0/c$ becomes constant. Choosing the z axis along the beam's direction, one can introduce the slowly varying amplitude $A(\mathbf{r})$ of the electric field as

$$\tilde{\mathbf{E}}(\mathbf{r},\omega_0) = \hat{\mathbf{p}}\, A(x,y,z)\, \exp(ikz), \tag{3}$$

where $\hat{\mathbf{p}}$ is a unit vector representing the beam's state of polarization. If we use Equation (3) in Equation (2) and neglect the second derivative $\partial^2 A/\partial z^2$ in the paraxial approximation, $A(x,y,z)$ is found to satisfy

$$2ik\frac{\partial A}{\partial z} + \frac{\partial^2 A}{\partial x^2} + \frac{\partial^2 A}{\partial y^2} = 0. \tag{4}$$

This equation governs the diffraction of CW beams in a homogeneous medium with the refractive index $n(\omega_0)$ at its frequency ω_0.

Spatial spreading of a CW beam depends on its initial spot size—narrower beams spread much more rapidly than wider beams [31]. If the spot size of a beam is elliptical such that its width is much wider in the y direction, the beam will mostly diffract in the x direction, and its size in the y direction will not change. The same thing happens when the beam is confined to a planar waveguide that guides it in the y direction. In both cases, the y derivative can be ignored in Equation (4) to obtain the following simpler equation:

$$\frac{\partial A}{\partial z} - \frac{i}{2k}\frac{\partial^2 A}{\partial x^2} = 0. \tag{5}$$

The situation is more complicated for a beam in the form of a short pulse with a relatively wide spectrum. In the most general case, diffraction and dispersion occur simultaneously, resulting in the so-called space–time coupling, and one must solve a four-dimensional problem. The problem is simplified considerably when such pulses are launched into a single-mode waveguide such as an optical fiber. In this case, the beam does not spread spatially because of its confinement, and we can focus on the dispersion-induced spreading of pulses in time.

To include the dispersive effects, we seek solutions of Equation (2) in the form

$$\tilde{\mathbf{E}}(\mathbf{r},\omega) = \hat{\mathbf{p}}\, F(x,y)\tilde{B}(z,\omega), \tag{6}$$

where $F(x,y)$ is the spatial form of the single mode supported by the waveguide. Using this form in Equation (2) and the resulting modal solution $F(x,y)$, $\tilde{B}(z,\omega)$ is found to satisfy

$$\frac{\partial^2 \tilde{B}}{\partial z^2} + \beta^2(\omega)\tilde{B} = 0, \tag{7}$$

where $\beta(\omega) = \bar{n}(\omega)\omega/c$ and $\bar{n}(\omega)$ is the effective index of the single mode.

Dispersive effects are included by expanding $\beta(\omega)$ in a Taylor series around ω_0 and retaining terms up to second order:

$$\beta(\omega) \approx \beta_0 + \beta_1\Omega + \frac{\beta_2}{2}\Omega^2, \tag{8}$$

where $\Omega = \omega - \omega_0$ and $\beta_m = (d^m\beta/d\omega^m)_{\omega=\omega_0}$ for $m = 0,1,2$. The parameter β_1 is related inversely to the group velocity, while β_2 governs its dispersion and is known as the group-velocity dispersion (GVD) parameter [33].

Similar to the CW case, one can introduce the slowly varying amplitude $\tilde{A}$ as $\tilde{B}(z,\omega) = \tilde{A}(z,\omega)\exp(i\beta_0 z)$. Neglecting its second derivative with respect to z, $\tilde{A}$ satisfies

$$2i\beta_0\frac{\partial \tilde{A}}{\partial z} + [\beta^2(\omega) - \beta_0^2]\tilde{A} = 0. \tag{9}$$

Using $\beta^2(\omega) - \beta_0^2 \approx 2\beta_0[\beta(\omega) - \beta_0]$ with the expansion in Equation (8), we obtain the simple differential equation

$$\frac{\partial \tilde{A}}{\partial z} = i\beta_1\Omega\tilde{A} + \frac{i\beta_2}{2}\Omega^2\tilde{A}. \tag{10}$$

This equation can be converted back to the time domain by using the inverse Fourier transform

$$A(z,t) = \frac{1}{2\pi}\int_{-\infty}^{\infty}\tilde{A}(z,\Omega)\,e^{-i\Omega t}\,d\Omega. \tag{11}$$

Noting that $-i\Omega\tilde{A}$ is the Fourier transform of $\frac{\partial A}{\partial t}$, Equation (10) in the time-domain takes the form

$$\frac{\partial A}{\partial z} + \beta_1 \frac{\partial A}{\partial t} + \frac{i\beta_2}{2}\frac{\partial^2 A}{\partial t^2} = 0. \tag{12}$$

The β_1 term in this equation can be eliminated using a reference frame moving with the pulse. Introducing $t' = t - \beta_1 z$ as a new time variable, we obtain

$$\frac{\partial A}{\partial z} + \frac{i\beta_2}{2}\frac{\partial^2 A}{\partial t'^2} = 0. \tag{13}$$

Equation (13) governs the dispersion-induced spreading of pulses in the time domain. It should be compared with Equation (5), which governs the dispersion-induced spreading of CW beams in space. The concept of space–time duality stems from the mathematical equivalence of these two equations. The parameter $1/k$ appearing in Equation (5) is replaced with the parameter $-\beta_2$ in Equation (13). While $k = 2\pi/\lambda_0$ is always positive, β_2 can be positive or negative, depending on the wavelength λ_0. The important point is that one should expect similar qualitative behavior to occur in the spatial and temporal cases. As an example, it is well known that a Gaussian beam maintains its Gaussian shape as it diffracts in space, even though its width changes because of diffraction [32]. The same statement can be made for Gaussian pulses dispersing and broadening in time inside a dispersive medium [33].

As another example of the usefulness of the concept of space–time duality, Figure 1a shows the diffraction pattern of a narrow slit. The solution of Equation (5) shows that $A(z,x)$ becomes the Fourier transform of the input field $A(0,x)$ (up to a phase factor) at a distance far from the plane $z = 0$, a feature known as the far-field diffraction [31]. As seen in Figure 1b, this feature implies that the shape of an optical pulse at the end of a long dispersive fiber would mimic the spectrum of that pulse [8]. As a result, time-domain measurements of a pulse's shape at the fiber's output can provide all frequency-domain information of the optical pulse launched into it. This technique, known as dispersive Fourier transform (DFT), provides single-shot spectra of optical pulses and has proven extremely useful in several areas that include biomedical imaging for observing in real time spectral changes occurring inside a medium [34–36].

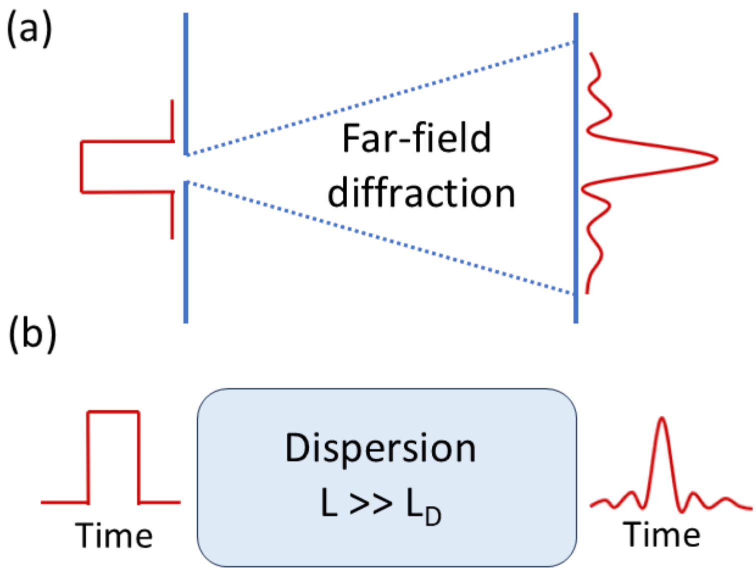

Figure 1. (**a**) The far-field diffraction pattern of a narrow slit providing Fourier transform of the input field. (**b**) The temporal analog showing that the shape of a pulse resembles its spectrum after a long dispersive medium.

3. Time Lens and Its Applications

As mentioned in the introduction, space–time duality was used as early as 1988 to develop the concept of a time lens and to use such lenses for temporal imaging [3–5]. A time lens may not resemble a conventional lens, but it performs the same function as a lens in the time domain. As seen in Figure 2a, a lens has curved surfaces such that its thickness changes along the transverse dimensions. When a plane wave passes through this lens, its phase front becomes curved because of a spatially varying phase shift $\phi_l(x, y)$ imposed by the lens that leads to its focusing. For a convex lens, this phase shift can be written as [32]

$$\phi_l(x, y) = kd_c - k(x^2 + y^2)/2f, \tag{14}$$

where d_c is central thickness of the lens of focal length f. Clearly, a time lens should add a time-dependent phase shift to the incoming pulse that varies as t^2. The important question is, what is the analog of the focal length for a time lens? To answer this and other related questions, let us solve Equation (13).

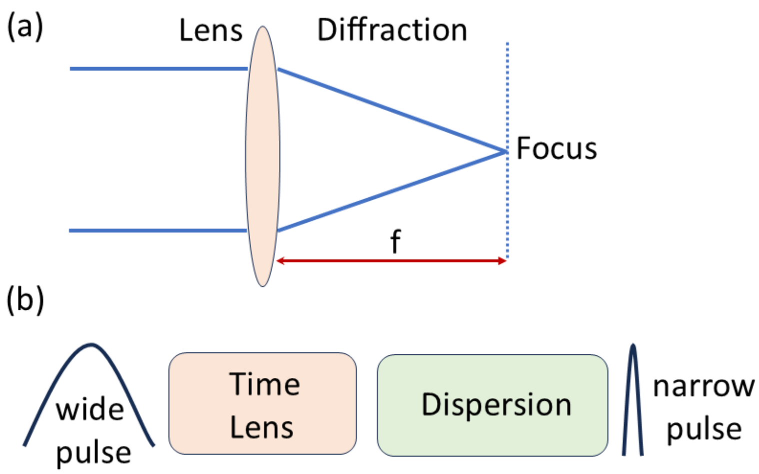

Figure 2. (**a**) The focusing of an optical beam by a lens. (**b**) The narrowing of a pulse by a time lens using a dispersive medium.

As Equation (13) is linear, we can solve it with the Fourier-transform method. Using the Fourier transform relation in Equation (11), $\tilde{A}$ satisfies an ordinary differential equation

$$\frac{\partial \tilde{A}}{\partial z} = \frac{i\beta_2}{2}\omega^2 \tilde{A}, \tag{15}$$

where we replaced Ω with ω for notational simplicity. Its solution is given by

$$\tilde{A}(z, \omega) = \tilde{A}(0, \omega) \exp\left(\frac{i}{2}\beta_2 z \omega^2\right). \tag{16}$$

Thus, GVD modifies the phase of each spectral component of the pulse by an amount that scales with frequency as ω^2. Even though such phase changes do not affect the optical spectrum, they can modify the pulse shape. It is useful to think of any dispersive medium of length L as a spectral filter and write Equation (16) in the form

$$\tilde{A}(L, \omega) = \tilde{A}(0, \omega)\tilde{h}(\omega), \qquad \tilde{h}(\omega) = \exp\left(\frac{i}{2}\beta_2 L \omega^2\right), \tag{17}$$

where $\tilde{h}(\omega)$ governs the action of this spectral filter.

By taking the inverse Fourier transform indicated in Equation (11), the solution of Equation (13) is found to be

$$A(L,t) = \frac{1}{2\pi}\int_{-\infty}^{\infty} \tilde{A}(0,\omega)\tilde{h}(\omega)e^{-i\omega t}\,d\omega, \tag{18}$$

where $\tilde{A}(0,\omega)$ is obtained from

$$\tilde{A}(0,\omega) = \int_{-\infty}^{\infty} A(0,t)e^{i\omega t}\,dt. \tag{19}$$

Evoking the convolution theorem, the preceding solution can also be written in the time domain as

$$A(L,t) = \int_{-\infty}^{\infty} h(t-t')A(0,t')\,dt', \tag{20}$$

where the impulse response of the filter $h(t)$ is obtained from

$$h(t) = \frac{1}{2\pi}\int_{-\infty}^{\infty} \tilde{h}(\omega)e^{-i\omega t}\,d\omega. \tag{21}$$

Using the form of $\tilde{h}(\omega)$ in Equation (17), the impulse response $h(t)$ is found to be

$$h(t) = (i\beta_2 L)^{-1/2}\exp\left(-\frac{it^2}{2\beta_2 L}\right), \tag{22}$$

where the frequency integration was carried out using

$$\int_{-\infty}^{\infty} \exp(-ax^2 \pm bx)\,dx = \sqrt{\frac{\pi}{a}}\exp\left(\frac{b^2}{4a}\right). \tag{23}$$

The impulse response in Equation (22) depends on a single parameter $D = \beta_2 L$, representing the net group-delay dispersion (GDD) over the medium's length L. This suggests that all properties of a dispersive medium should depend on D, including the temporal analog of the focal length of a lens. Thus, the phase shift imposed by a time lens, the temporal analog of Equation (14), should have the form [9]

$$\phi_l(t) = \phi_0 + t^2/2D_f, \tag{24}$$

where ϕ_0 is a constant phase and D_f is the focal GDD of the time lens. A time-varying phase can be related to the frequency chirp imposed on the pulse. Using $\delta\omega(t) = -(d\phi_l/dt)$, a quadratic time dependence implies a linear chirp $\delta\omega(t) = -t/D_f$.

The device used in 1988 as a time lens was a phase modulator [3]. Such devices impose a sinusoidal phase shift on an optical wave, when a microwave signal is used to modulate the refractive index of a suitable electro-optic material, such as a lithium niobate ($LiNbO_3$) crystal (or waveguide). In this situation, the input and output fields are related as

$$A_{\text{out}}(t) = A_{\text{in}}(t)\exp[i\phi_m\cos(2\pi f_m t + \theta)], \tag{25}$$

where ϕ_m is the maximum phase shift, f_m is the modulation frequency, and θ is a phase that depends on how the modulator is biased. Choosing this phase as $\theta = \pi$, and expanding the cosine function in a Taylor series around $t = 0$, we obtain

$$A_{\text{out}}(t) = A_{\text{in}}(t)\exp[-i\phi_m + \tfrac{1}{2}\phi_m(2\pi f_m)^2 t^2]. \tag{26}$$

Thus, a short pulse whose intensity peaks at $t = 0$ undergoes a phase shift in the form given in Equation (14) such that $D_f = (4\pi^2 \phi_m f_m^2)^{-1}$. The phase shift is quadratic only if the pulse width T_0 is considerably shorter than the modulation period $1/f_m$. For a modulator operating at 10 GHz, T_0 should not exceed 10 ps. Several nonlinear techniques have been used in recent years for making time lenses with improved properties [9].

Consider the temporal analog of focusing shown in Figure 2b. In the temporal case, a relatively wide pulse is chirped first by a time lens and then transmitted through a dispersive medium whose length is chosen to satisfy the relation $D = \beta_2 L = D_f$. In this case, the output field is obtained from Equation (20) using $A(0,t) = A_p(t)\exp(it^2/2D_f)$, where $A_p(t)$ governs the pulse shape and the quadratic phase is imposed by the time lens. The integration can be conducted for Gaussian-shape pulses. Using $A_p(t) = A_0 \exp(-t^2/2T_0^2)$, the input can be written in the form of a chirped Gaussian pulse as

$$A(0,t) = A_0 \exp\left[-\frac{1+iC}{2}\left(\frac{t}{T_0}\right)^2\right], \tag{27}$$

where the chirp parameter $C = -(T_0^2/D_f)$ is negative and T_0 is related to the full-width at half-maximum of the pulse as $T_p = 1.665T_0$. By taking the Fourier transform of $A(0,t)$, we obtain

$$\tilde{A}(0,\omega) = A_0\left(\frac{2\pi T_0^2}{1+iC}\right)^{1/2} \exp\left[-\frac{\omega^2 T_0^2}{2(1+iC)}\right]. \tag{28}$$

The propagation of a chirped Gaussian pulse through a dispersive medium has been studied in the context of fiber-optic communication systems [33]. Substituting Equation (28) into Equation (18) and using Equation (23), frequency integration can be performed to obtain:

$$A(L,t) = \frac{A_0}{\sqrt{Q}} \exp\left[-\frac{(1+iC)t^2}{2T_0^2 Q}\right], \tag{29}$$

where $Q = 1 + (C - i)\beta_2 L/T_0^2$. This equation shows that a Gaussian pulse remains Gaussian on propagation, but its width, chirp, and amplitude change as dictated by the factor Q. Specifically, the chirp changes from its initial value C to become $C_1 = C + (1 + C^2)\beta_2 L/T_0^2$. The width of the output pulse becomes minimum when the pulse becomes unchirped. Using $C_1 = 0$ with $C = -(T_0^2/D_f)$ and $D = \beta_2 L = D_f$, this condition is reduced to

$$D = \frac{D_f T_0^4}{D_f^2 + T_0^4} \approx D_f, \tag{30}$$

assuming that $D_f \ll T_0^2$. At the focal distance, the pulse is compressed by a factor of $|Q|$. It is easy to show that the minimum width of the pulse is given by $T_{\min} = D/T_0$. Pulses can be compressed by a large factor by a time lens for small values of the ratio D_f/T_0^2.

Spatial lenses are used routinely for imaging in devices such as cameras and microscopes. In the simplest situation, a single lens of focal length f images an object placed at a distance s_1 on its one side. The image may be magnified (or reduced) and is produced at a distance s_2 that satisfies the following imaging condition:

$$\frac{1}{s_1} + \frac{1}{s_2} = \frac{1}{f}. \tag{31}$$

Time lenses were used for time-domain imaging starting in 1988 and follow an analogous scheme. The object takes the form of a time-varying signal. This signal is passed through a dispersive medium with $D_1 = \beta_2 L_1$, before it is chirped by a time lens with the focal GDD D_f. Its imaging occurs when the chirped signal passes though a second dispersive medium with $D_2 = \beta_2 L_2$. As one would expect from space–time duality, the imaging condition satisfies a relation that is identical to that in Equation (31):

$$\frac{1}{D_1} + \frac{1}{D_2} = \frac{1}{D_f}. \tag{32}$$

Other imaging properties such as magnification factor follow the same duality scheme. One application of temporal imaging is to stretch ultrashort pulses so much that their shape can be measured using a photodetector. It is important to mention that higher-order dispersion terms, neglected in Equation (8), can produce "imaging abberations" for ultrashort pulses. As the applications of time lenses related to imaging and optical signal processing have been discussed in several past reviews [7–9], I focus on more recent advances in what follows.

4. Temporal Reflection and Refraction

Wave propagation in a dielectric medium whose refractive index varies spatially has been studied for a long time, as it is useful for analyzing optical components such as graded-index fibers [21], Bragg gratings [22], and photonic crystals [23]. Recent attention to time-varying media [24–26], where the refractive index varies with time, constitutes a new example of space–time duality. Even though the phenomena covered in the next few sections extend the original concept considerably, and some may prefer to call them analogs, I like to unite them under the umbrella of space–time duality.

4.1. Temporal Boundary in a Dispersive Medium

The simplest situation occurs when the refractive index is changed suddenly at a specific time in a spatially uniform fashion, resulting in a boundary that is the temporal analog of the spatial interface between two dielectric media. Just as the reflection and refraction of an optical beam occurs at a spatial interface, optical pulses must experience the temporal analog of these two phenomena [13–15]. As it is difficult to produce rapid index changes all across a medium on femtosecond time scales, experiments have involved low frequencies using water waves or microwaves [37,38]. Further, effects of chromatic dispersion should be included for any dielectric medium with a time-varying refractive index.

It turns out that these issues can be addressed with the technique of traveling-wave modulation, which changes the refractive index of a dispersive medium in a region that moves at a constant speed [16]. The simplest case, shown schematically in Figure 3, corresponds to a moving boundary (thick black line) with different refractive indices on its two sides. When an optical pulse interacts with this boundary inside a dispersive medium, it splits into two parts, whose frequencies are shifted such that they travel at different speeds [17–20]. These two parts correspond to transmitted and reflected pulses and are temporal analogs of the reflection and refraction at a spatial interface [15].

One should ask why temporal reflection requires a frequency shift of pulses, whereas spatial reflection manifests as a change in the direction of the propagation of the incident beam. The answer is related to the conservation law that must be satisfied. At a spatial interface, space translation symmetry is broken. As a result, the energy of the photons is conserved, but their momenta are not. Recall that a photon's momentum depends on its direction of propagation. This is why reflected and refracted waves propagate in directions different from that of the incident wave. At a temporal boundary, time translation symmetry is broken. Thus, we expect the momentum to be conserved, but the energy of the photons can change. As a photon's energy $\hbar\omega$ depends on the wave's frequency, it is the frequency of an incoming wave that changes during temporal reflection and refraction [13].

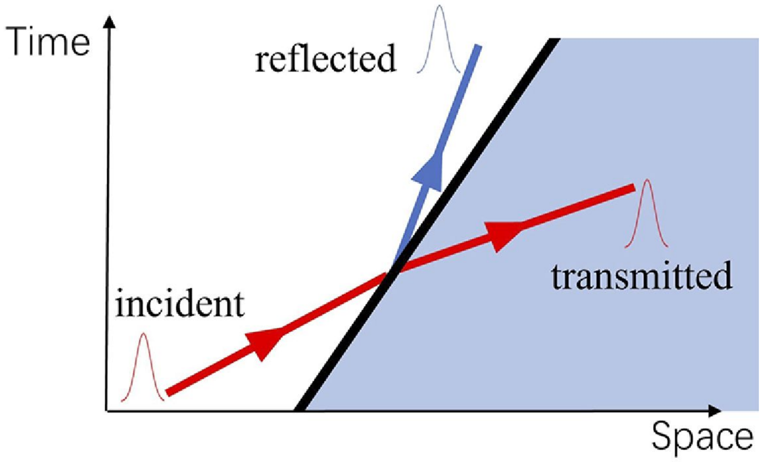

Figure 3. The temporal analogs of reflection and refraction at a temporal boundary (tilted black line) with different refractive indices on its two sides. Arrows indicate the incident, reflected, and transmitted waves.

In the case of a moving index boundary, both translation symmetries are broken, and neither energy nor momentum is conserved. However, in a moving frame in which index modulation becomes stationary, the refractive index does not depend on the spatial coordinate z. As the space translation symmetry is preserved in this frame, momentum of all photons is conserved. Noting that the momentum of a photon of energy $\hbar\omega$ is related to the propagation constant as $\hbar\beta(\omega)$ at any frequency, $\beta(\omega)$ must remain conserved at all frequencies. This requirement can be used to study how the wavelength of a probe pulse changes as it propagates through a time-varying medium [15].

4.2. Mathematical Model

We can use the propagation of Equation (12) for studying temporal reflection by adding a term to its right side representing the impact of a moving temporal boundary:

$$\frac{\partial A}{\partial z} + \beta_1 \frac{\partial A}{\partial t} + \frac{i}{2}\beta_2 \frac{\partial^2 A}{\partial t^2} = i\beta_b u(t - z/v_m)A, \tag{33}$$

where $\beta_b = k_0 \delta n$, δn is the index change at the temporal boundary moving at the speed v_m, and $u(t)$ is the step function. It is useful to work in a frame in which boundary appears stationary. Introducing a new time variable as $T = t - z/v_m$, Equation (33) becomes

$$\frac{\partial A}{\partial z} + \Delta\beta_1 \frac{\partial A}{\partial T} + \frac{i\beta_2}{2} \frac{\partial^2 A}{\partial T^2} = i\beta_b u(T)A, \tag{34}$$

where $\Delta\beta_1 = \beta_1 - 1/v_m$ is related to speed of the pulse relative to that of the boundary. This equation is useful for studying a wide variety of spatiotemporal effects occurring inside a dispersive medium. It is linear because probe pulses are assumed to be not too energetic. For intense pulses, a nonlinear term of the form $i\gamma|A|^2 A$ should be added to this equation [10].

Even without the nonlinear term, Equation (34) resembles the NLS equation because of the time-dependence of the last term. For this reason, it can be solved numerically with the same techniques used for solving the NLS equation. One such technique, known as the split-step Fourier method, alternates between the time and frequency domains for including the modulation and dispersive effects, respectively, [10]. Another technique converts Equation (34) to the frequency domain and employs the Runge–Kutta algorithm. We refer to Ref. [10] for further details.

Before solving Equation (34) numerically, it is useful to introduce normalized variables as $\tau = T/T_0$ and $\xi = z/L_D$, where T_0 is related to the width of input pulses and $L_D = T_0^2/|\beta_2|$ is the dispersion length. The resulting equation becomes

$$\frac{\partial A}{\partial \xi} + d\frac{\partial A}{\partial \tau} + \frac{i\,s}{2}\frac{\partial^2 A}{\partial \tau^2} = iC_b u(\tau)A \tag{35}$$

where $d = \Delta\beta_1 L_D$, $s = \mathrm{sgn}(\beta_2)$, and $C_b = \delta n(k_0 L_D)$ are three dimensionless parameters. In the moving frame, the temporal boundary remains at $\tau = 0$.

As an example of temporal reflection and refraction in a dispersive medium, Figure 4 shows the results obtained by solving Equation (35) numerically using $d = 20$, $s = 1$, and $C_b = 100$, values appropriate for a silica fiber [15]. The probe pulse at the input end is assumed to have a Gaussian shape such that $A(0,\tau) = A_0 \exp[-\frac{1}{2}(\tau - \tau_s)^2]$ with $\tau_s = -5$. Temporal evolution shows how the pulse splits into its reflected and refracted parts when it arrives at the boundary (vertical dashed line) where the refractive index increases by a small amount ($< 10^{-7}$ for the parameter values used). Both parts experience frequency shifts such that their spectra are red-shifted). The magnitude of frequency shift is small for the transmitted pulse but exceeds $6/T_0$ for the reflected pulse. The reflected part does not cross the boundary because of its much larger frequency shift. Blue shifts can occur when β_2 is negative at the wavelength of probe pulses.

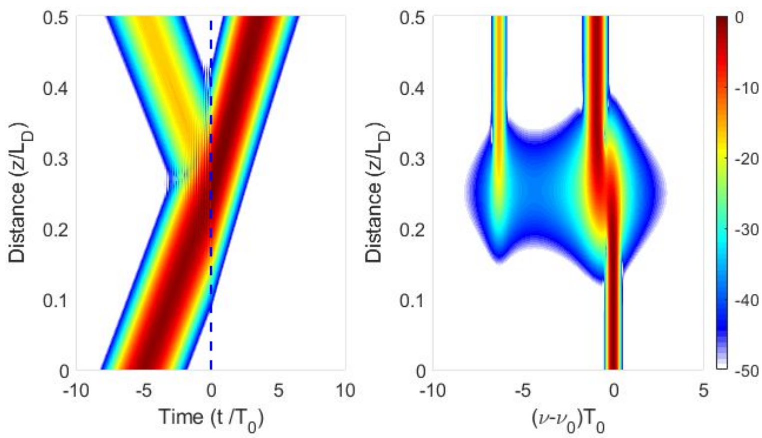

Figure 4. The temporal reflection and refraction of a Gaussian pulse at a temporal boundary fixed at $\tau = 0$ (dashed line) in the moving frame. Spectra show frequency shifts occurring for the two processes. In both cases, colors show intensity variations on a 50 dB scale.

Spectral shifts can be calculated by invoking the conservation of momentum in the moving frame in which boundary is stationary. This requires $\beta(\omega)$ to remain unchanged for the reflected and transmitted parts from its initial value at every frequency within the probe's spectrum. Let Ω_r and Ω_t be the frequency shifts when the probe's frequency is $\omega_0 + \Omega$. The conservation of momentum provides the following expression for these two shifts [15,19],

$$\Omega_r = -\Omega - (2\Delta\beta_1/\beta_2). \tag{36}$$

$$\Omega_t = -\frac{\Delta\beta_1}{\beta_2} + \frac{1}{\beta_2}[(\Delta\beta_1 + \beta_2\Omega)^2 - 2\beta_b\beta_2]^{1/2}. \tag{37}$$

It is remarkable that both frequency shifts do not depend on the probe's parameters. They can be positive or negative (blue or red shifts) depending on the signs of the fiber's parameters involved.

It is possible to obtain analytic expressions for the reflection and transmission coefficients at a given frequency. By matching the boundary conditions on the two sides of the temporal boundary, these are found to depend on the frequency shifts given in Equations (36) and (37) as follows [19]:

$$R(\Omega) = \frac{\Omega_t - \Omega}{\Omega_r - \Omega_t}, \quad T(\Omega) = \frac{\Omega_r - \Omega}{\Omega_r - \Omega_t}. \tag{38}$$

4.3. Time-Domain Total Internal Reflection

The expression in Equation (37) indicates the possibility of total internal reflection (TIR) of the probe pulse at a moving boundary. To see this clearly, let us focus on the central frequency of the pulse and set $\Omega = 0$ in Equation (37) to obtain

$$\Omega_t = -\frac{\Delta\beta_1}{\beta_2} + \frac{1}{\beta_2}[(\Delta\beta_1)^2 - 2\beta_b\beta_2]^{1/2}. \tag{39}$$

For small values of index change, frequency shifts are real. However, Ω_t becomes a complex quantity when δn is large enough to satisfy the relation $2\beta_b\beta_2 > (\Delta\beta_1)^2$. In this situation, only a reflected pulse is produced at a shifted wavelength. This temporal analog of TIR differs from the conventional TIR in one respect. While spatial TIR requires light to travel from a high-index region to a low-index one, temporal TIR has no such restriction. This is because the dispersion parameter β_2 in Equation (43) can take both positive and negative values, depending on the wavelength of incident light. When β_b is negative, β_2 should also be negative for the TIR to occur.

As an example of TIR, numerical results shown in Figure 5 were obtained under the same conditions used for Figure 4, except that the value of C_b was larger by a factor of three. As seen there, the probe pulse undergoes TIR at the temporal boundary (vertical dashed line), and its spectrum shifts by more than $6/T_0$. The index change required for this phenomenon to occur is less than $\times 10^{-6}$ at probe wavelengths near 1 μm. Simulations show that, similar to the spatial case, an evanescent wave exists on the other side of the temporal boundary.

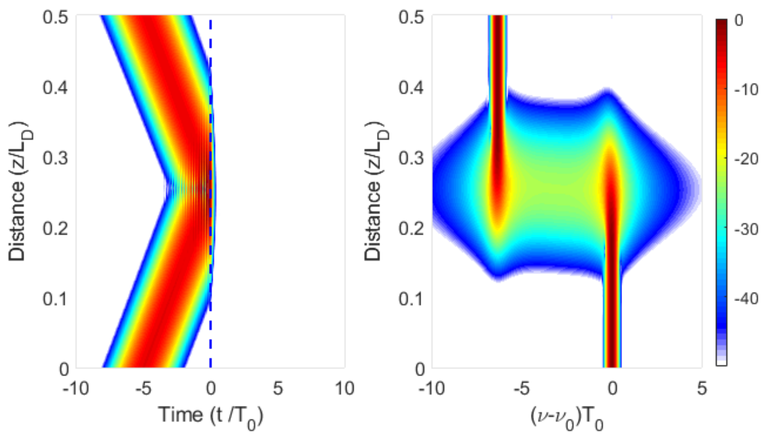

Figure 5. TIR of a Gaussian pulse in the time domain. The figure was produced under the same conditions as Figure 4 except for a larger index change at the boundary ($C_b = 300$).

In the case of a spatial interface, TIR is accompanied with the Goos–Hänchen effect, which corresponds to a shift of the reflected beam's center relative to its position expected for normal reflection. Based on the concept of space–time duality, such a shift to occur in the temporal case as well. It was found in 2022 that this is indeed the case [39]. The following analytic expression provides a temporal shift of the TIR pulse:

$$\Delta\tau_{\mathrm{GH}} = \frac{2\,\mathrm{sgn}(\Delta\beta_1)\beta_2}{\sqrt{2\beta_b\beta_2 - (\Delta\beta_1)^2}}. \tag{40}$$

Numerical simulations based on Equation (34) show clearly such a temporal shift. As an example, a 6 ps wide Gaussian pulse undergoing TIR inside an optical fiber was found to exhibit a Goos–Hänchen shift of about 0.52 ps. This shift agrees well with the predicted value based on Equation (40) for the parameter values used for simulations.

5. Solitons as Moving Boundaries

A moving index boundary can be realized using the optical Kerr effect. In this case, intense pump pulses are launched into a nonlinear dispersive medium, such as an optical fiber [10]. Owing to the Kerr effect, the fiber's refractive index increases with intensity by a small amount $n_2 I$, where n_2 is the Kerr coefficient. Thus, pump pulses increase the refractive index in a time window set by their width, and this window moves at the speed of pump pulses. When a probe pulse, moving at a different speed because of its different wavelength, interacts with this index window, a reflected pulse is generated at a wavelength shifted from that of the probe [18].

In general, pump pulses launched into an optical fiber become distorted because of the dispersive and nonlinear effects, resulting in a high-index region that does not maintain itself over the fiber's length. This problem can be solved by making use of optical solitons, forming when pump pulses are launched at a wavelength longer than the zero-dispersion wavelength of the fiber so that the GVD is anomalous at the pump's wavelength [10]. Formation of solitons requires that the width and peak power (T_s and P_s) of pump pulses are chosen such that $N^2 = \gamma_p P_s T_s^2/|\beta_{2p}| = 1$, where N is the soliton's order and β_{2p} is the GVD a the pump's wavelength. The nonlinear parameter γ_p is related to the Kerr coefficient n_2 as $\gamma_p = \omega_p n_2/(cA_{\text{eff}})$, where A_{eff} is the effective area of the single mode supported by the fiber.

The shape of the soliton inside the fiber does not change under such conditions, and its power varies with time as $P(t) = P_s \operatorname{sech}^2(T/T_s)$. The fiber's refractive index n increases by a small amount (typically $< 10^{-6}$) over the soliton's duration and is the largest at the peak of the soliton. This increase in n creates a spatiotemporal boundary, moving at the speed of pump pulses. A probe pulse sees this increase through $\beta_b = 2\gamma P(t)$, where γ is the probe's nonlinear parameter [10]. The factor of two results from the nonlinear phenomenon of cross-phase modulation (XPM).

5.1. Soliton-Induced Temporal Reflection

The probe's evolution is governed by Equation (34) after $\beta_b u(T)$ on its right side is replaced by the XPM term as follows:

$$\frac{\partial A}{\partial z} + \Delta\beta_1 \frac{\partial A}{\partial T} + \frac{i\beta_2}{2}\frac{\partial^2 A}{\partial T^2} = 2i\gamma P_s \operatorname{sech}^2(T/T_s)A. \tag{41}$$

This equation can be written in a normalized form of Equation (35) as

$$\frac{\partial A}{\partial \xi} + d\frac{\partial A}{\partial \tau} + \frac{i\,s}{2}\frac{\partial^2 A}{\partial \tau^2} = iC_x \operatorname{sech}^2(\tau/\tau_s)A, \tag{42}$$

where $\tau_s = T_s/T_0$ and $C_x = 2\gamma P_s L_D$. The parameter τ_s compares the soliton's width to that of the probe. The parameter C_x governs the XPM-induced interaction between the two pulses. This equation can be solved numerically to study the interaction of a probe pulse with a pump soliton inside a dispersive fiber. In the moving fame, the soliton's peak remains fixed at $\tau = 0$.

When a soliton is used to form a moving boundary, the refractive index increases only over its duration. The situation differs considerably from that of a sharp boundary discussed in Section 4.2 because a soliton provides two interfaces at its leading and trailing edges with finite rise and fall times. In spite of this, temporal reflection exhibits similar features in the two cases. As an example, Figure 6 shows the temporal reflection and refraction of a Gaussian pulse from a soliton 10 times narrower than the pulse ($\tau_s = 0.1$) using $d = 20$ and $C_x = 300$. Time-domain TIR occurs for values of C_x larger than 400. The impact of a boundary's sharpness on temporal reflection was studied in 2021 using a transfer-matrix approach with a staircase model [20]. The results show that TIR persists even for shallow boundaries with long rise times.

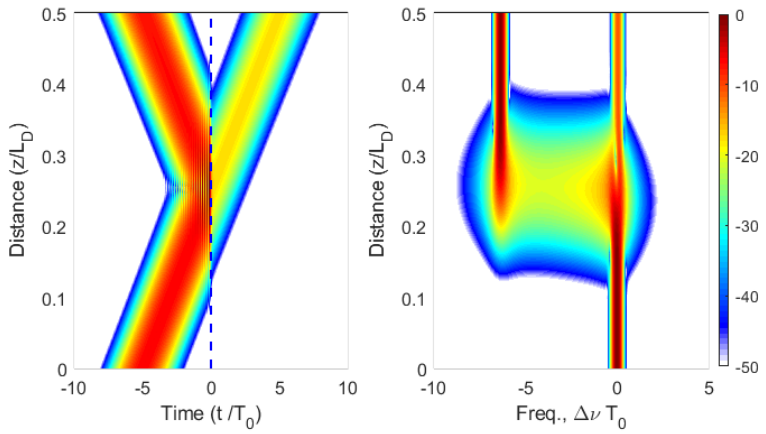

Figure 6. The same as Figure 4, except that a soliton 10 times shorter than the pulse plays the role of the temporal boundary. A dashed vertical line marks the location of the soliton's peak in the moving frame.

It turns out that the reflectivity of a soliton can be found in an analytic form with a simple trick. We can remove the second term in Equation (41) by shifting ω_0 from the probe's central frequency to the one for which $d = 0$. With this shift in the reference frequency, Equation (42) takes the form of the Schrödinger equation:

$$i\frac{\partial A}{\partial \xi} = \frac{s}{2}\frac{\partial^2 A}{\partial \tau^2} + V(\tau)A. \tag{43}$$

where $A(\xi, \tau)$ is the wave function and $V(\tau) = -C_x \text{sech}^2(\tau/\tau_s)$ plays the role of a potential barrier. Notice that ξ plays the role of time and τ plays the role of a spatial coordinate. Even though Equation (43) does not contain $\hbar$, as expected for a classical problem, it is useful because one can use relevant quantum results with only minor changes. It shows that the time-reflection problem is analogous to the scattering of a quantum particle from a potential barrier. This analogy is another type of space–time duality where the time evolution of a quantum particle is mapped to the spatial evolution of optical waves.

The observation of temporal reflection from a soliton requires a short pump pulse and a probe pulse traveling at nearly the same speed at a different wavelength. In a 2012 experiment [40], performed using a short microstructured fiber (only 1.1 m long), the zero-dispersion wavelength of the fiber was near 710 nm. This feature allowed the use of 105 fs pulses, emitted by a Ti–sapphire laser operating at 810 nm. Each pulse was launched such that it formed an optical soliton in the anomalous-GVD region of the fiber. Probe pulses were launched in the normal-GVD region of the fiber at wavelengths near 620 nm and traveled at nearly the speed of pump pulses. When the wavelength of probe pulses was varied from 595 to 645 nm, either a blue shift or a red shift was observed for the "reflected" pulse at the output end of the fiber, depending on whether the probe was traveling slower or faster than the soliton. The observed frequency shifts matched predictions based on Equation (38).

5.2. Time-Domain Waveguides

Optical waveguides are devices that confine light spatially to their core region through TIR at the core-cladding interfaces [32,41]. Similarly to the spatial case, time-domain TIR can be used to provide the temporal analog of optical waveguides. In the temporal case, a pulse would be confined within a moving time window, where the refractive index differs from the regions outside of that window [17]. When a probe pulse is located in the middle of two fundamental solitons acting as mirrors, it travels first toward one of these solitons and is totally reflected from it. The spectrum of the reflected pulse is shifted such that it slows down and moves away from this soliton. When the pulse arrive at the second soliton, it is reflected again through TIR, and its center frequency shifts back to the original value. This process repeats itself, trapping the pulse between the two solitons.

Figure 7 reveals how such a waveguide functions by solving Equation (42) numerically, after it was modified to include the impact of both solitons:

$$\frac{\partial A}{\partial \xi} + d\frac{\partial A}{\partial \tau} + \frac{i\,s}{2}\frac{\partial^2 A}{\partial \tau^2} = iC_x\left[\mathrm{sech}^2\left(\frac{\tau - q}{\tau_s}\right) + \mathrm{sech}^2\left(\frac{\tau + q}{\tau_s}\right)\right]. \tag{44}$$

It shows the temporal (left) and spectral (right) evolution along the length of a dispersive medium when a Gaussian-shaped probe pulse of width T_0 is located initially in the middle of two solitons, separated by $10\,T_0$. In normalized units, Equation (44) was solved with the initial amplitude $A(0,\tau) = \exp(-\tau^2/2)$ using parameter values $d = 40$, $s = 1$, $\tau_s = 0.1$, and $C_x = 1800$. Two solitons, with their peaks located at $q = \pm 5$ (vertical dashed lines in Figure 7), were 10 times shorter than T_0. As expected, the spectrum of pulse confined within the waveguide's core shifts back and forth after TIR occurring at the high-index boundaries provide by two solitons. As a practical example, when $T_0 = 5$ ps for probe pulses at a wavelengths near 1.1 µm, the required fiber's length is around 1 km. The wavelength of 0.5 ps pump pulses should be near 1.5 μm to ensure anomalous GVD needed for the two solitons.

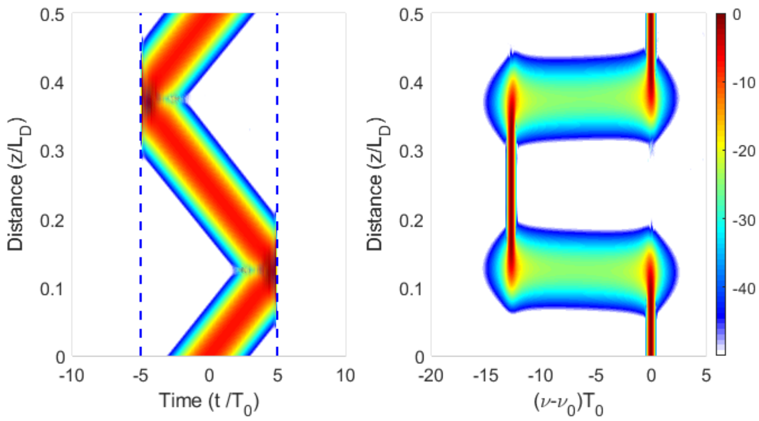

Figure 7. The evolution of the shape (left) and spectrum (right) of a Gaussian pulse inside a temporal waveguide formed by two solitons acting as high-index boundaries where TIR can occur. Vertical dashed lines mark the core region of this waveguide.

It is important to emphasize that the solitons are not essential for making temporal waveguides. A waveguide is formed whenever two boundaries form a time window where the refractive index differs from that outside the window. One should analyze whether such waveguides support temporal modes that are analogous to the spatial modes of planar waveguides. Modifying the right side of Equation (34) to include the two boundaries located at $T = \pm T_b$, we obtain

$$\frac{\partial A}{\partial z} + \Delta\beta_1 \frac{\partial A}{\partial T} + \frac{i\beta_2}{2}\frac{\partial^2 A}{\partial T^2} = i\beta_b[u(T+Tb) - u(T-Tb)]A. \tag{45}$$

To find the temporal modes, we look for solutions of Equation (45) within the time window $-T_b < T < T_b$ in the form

$$A(z,T) = M(T)\exp[i(Kz - \Omega T)], \tag{46}$$

where $M(T)$ is the temporal shape of the mode, K is the eigenvalue for this mode, and Ω is a frequency shift occurring because of the $\Delta\beta_1$ term in Equation (45).

Substituting Equation (46) into Equation (45) and equating the real and imaginary parts, we obtain

$$(\Delta\beta_1 + \beta_2\Omega)\frac{dM}{dT} = 0, \tag{47}$$

$$\frac{d^2M}{dT^2} + \frac{2}{\beta_2}\left(K - \Omega\Delta\beta_1 - \frac{\beta_2\Omega^2}{2} - \beta_b\right)M = 0. \tag{48}$$

From Equation (47), the frequency shift for all modes is found to be $\Omega = -\Delta\beta_1/\beta_2$. Using this value of Ω in Equation (48), the modes are found by solving

$$\frac{d^2M}{dt^2} + \frac{2}{\beta_2}\left(K + \frac{(\Delta\beta_1)^2}{2\beta_2} - \beta_b\right)M = 0. \tag{49}$$

This eigenvalue equation provides temporal shapes of modes for specific eigenvalues K.

At this point, one can follow the same procedure used for spatial waveguides to find the temporal profiles of different modes [17]. Similarly to the spatial case, one can introduce a dimensionless parameter as

$$V = \sqrt{(2\beta_b T_b^2)/\beta_2}. \tag{50}$$

This parameter determines the number of modes supported by a temporal waveguide of width $2T_b$. In analogy with the spatial case, the waveguide supports m modes when $V < (m+1)\pi/2$. In particular, a temporal waveguide supports only a single mode ($m = 0$) if it is designed such that $V < \pi/2$.

A clear evidence of the formation of a temporal waveguide by two solitons was seen in a 2015 experiment through a pump–probe type experiment [42]. A 29 m long photonic crystal fiber was employed with its zero-dispersion wavelength near 980 nm. Pump pulses were 250 fs wide, and their wavelength was tunable from 1000 to 1500 nm. Probe pulses were considerably wider, and their 802 nm wavelength was in the normal-GVD region of the fiber. Each pump pulse was split into two pulses, separated by 3.6 ps, using the setup similar to a Michelson interferometer. Probe pulses were synchronized such that each was located in the center of a pair of pump pulses at the input end of the fiber.

5.3. Temporal Fabry–Perot Resonators

A conventional Fabry–Perot resonator (FPR) consists of two partially reflecting mirrors enclosing a medium of constant refractive index n. The transmission spectrum of such a device is in the form of a frequency comb and exhibits a periodic resonances occurring at frequencies $\nu_m = mc/(2nL_r)$, where m is an integer and L_r is the resonator's length. Such devices are routinely used for spectral analysis in many applications. As we have seen, solitons inside an optical fiber act effectively as mirrors in the time domain. One can construct the temporal analog of an FPR by using two such solitons separated in time by constant interval. Such a device was analyzed in a 2021 study using a matrix approach [43].

When a probe pulse is incident at such an FPR, it can be transmitted or reflected, depending on whether its spectrum falls within or outside of a resonance peak. Figure 8 shows this behavior for an FPR made with two 80 fs solitons, separated by 1.4 ps. The temporal evolution of a relatively wide Gaussian pulse (width 20 ps) was simulated numerically in two cases. The probe's spectrum fits within a transmission peak in case (a) but falls in between two peaks in case (b). Part (d) shows the location of the pulse's spectrum in the two cases within the transmission spectrum of the FPR. Time-varying index changes induced by two solitons are shown in part (c). As expected, the probe pulse is transmitted when its spectrum falls within a transmission peak. In contrast, it is mostly reflected when its spectrum falls in the middle of two transmission peaks. Experimental observation of a such a soliton-based time-domain FPR was lacking at the time of writing but would be of considerable interest.

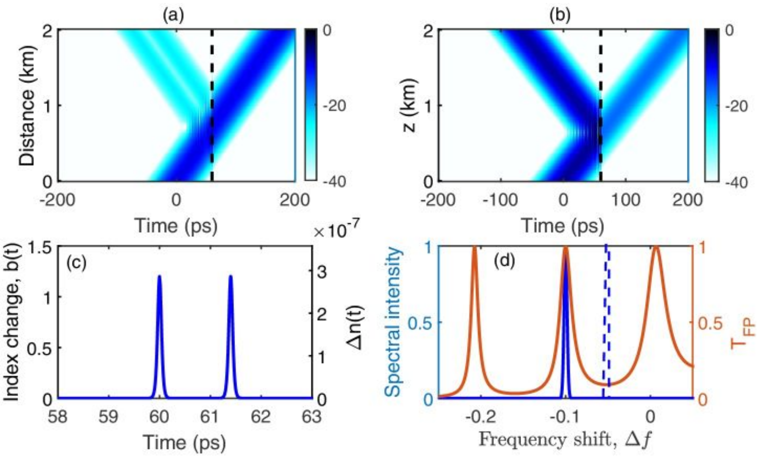

Figure 8. The temporal evolution of a 20 ps Gaussian pulse when its spectrum is (**a**) centered at a transmission peak and (**b**) falls outside of it. (**c**) An index change induced by solitons. (**d**) The location of the pulse's spectra within the transmission spectrum. Adapted with permission from [43] © Optica Publishing Group.

6. Periodic Index Variations

Wave propagation in a medium whose refractive index varies spatially has a long history. When the refractive index varies in the transverse directions only, it is useful for making optical waveguides such as graded-index fibers [21]. In the opposite limit, where the refractive index varies periodically along the direction of propagation, devices such as Bragg gratings [22] and photonic crystals [23] have found a multitude of applications.

The concept of space–time duality suggests that wave propagation in a medium whose refractive index varies with time should exhibit novel features with useful applications. Recent studies of time-varying media have shown that this is indeed the case [24–26]. The specific situation in which the medium's refractive index varies periodically along the direction of propagation has led to novel concepts such as photonic time crystals [27–29] and temporal Bragg gratings [30,44]. Two cases should be distinguished in practice. In one case, periodic index variations must occur over the entire length of the medium on the time scale of a single cycle. In the second case, index variations occur in a section of the medium that moves at a finite speed. The later scheme is easier to implement because it allows index changes to occur on a longer time scale (but shorter than pulses involved). Further, dispersive effects must be included. We consider the second case first.

6.1. Spatiotemporal Bragg Gratings

As we saw in Section 5, a single soliton acts as a time-domain mirror, and two such mirrors can be used for making a time-domain waveguide. The temporal analog of a Bragg grating occurs when multiple solitons inside a dispersive medium, equally separated in time, act as partially reflecting mirrors. However, as solitons are moving at the speed of pump pulses, the Bragg grating also moves at the same speed inside the medium containing these solitons. The properties of such spatiotemporal Bragg gratings (STBGs) were studied recently [30]. The case of a non-moving Bragg grating was considered in Ref. [44] without including the dispersive effects of the medium.

In the case of a spatial index modulation, Bragg gratings exhibit a photonic band gap in the energy or frequency domain, centered at the Bragg frequency set by the period of index modulation. In contrast, as is well known, temporal periodicity of the refractive index produces momentum (or wave-number) gaps in the band structure of a photonic time crystal [27–29]. This is expected from the discussion of space–time duality if we recall that energy and momentum conservation laws are switched in the space and time domains. In contrast to spatial crystals, which exhibit energy gaps in their band structure, photonic time crystals exhibit momentum gaps in their band structure.

We can find momentum gaps by replacing Equation (42) with

$$\frac{\partial A}{\partial \xi} + \frac{i\,s}{2}\frac{\partial^2 A}{\partial \tau^2} = \frac{iC_x}{\tau_1^2}\sum_m \operatorname{sech}^2\left(\frac{\tau - m}{\tau_1}\right)A, \tag{51}$$

where the sum is over all pulses within the soliton train and two neighboring solitons of width T_s are separated in time by T_d such that $\tau_1 = T_s/T_d$. The parameter $\tau = T/T_d$ is normalized using this separation (and not the width T_s). The d term in Equation (42) was removed by choosing the reference frequency as the frequency for which $\Delta\beta_1$ vanishes. The preceding equation has the same mathematical form as the Schrödinger equation for an electron moving in a periodic potential. Using $A(\xi, \tau) = e^{i\kappa\xi}B(\tau)$ with $s = 1$, we can write it as an eigenvalue problem with a suitable Hamiltonian:

$$\hat{H}B = \kappa B, \qquad \hat{H} = -\frac{1}{2}\frac{d^2}{d\tau^2} + V(\tau), \tag{52}$$

where $V(\tau)$ is the periodic potential on the right side of Equation (51). Notice that ξ plays the role of time and κ is the analog of energy in quantum mechanics.

From the Floquet theorem, $B(\tau)$ has the form $B(\tau) = e^{-i\Omega\tau}\bar{A}(\tau)$, where Ω is the Floquet frequency and $\bar{A}(\tau)$ is a periodic function with the period τ_p of the soliton train ($\tau_p = 1$ in normalized units). We only need to solve Equation (52) in the interval $[0, \tau_p]$. For given values of B and $B' = dB/d\tau$ at one end, this equation provides the values of B and B' at the other end in the form

$$\begin{pmatrix} B(\tau_p) \\ B'(\tau_p) \end{pmatrix} = M \begin{pmatrix} B(0) \\ B'(0) \end{pmatrix}, \tag{53}$$

where the elements of transfer matrix M are found by solving Equation (52) two times with the initial conditions (i) $B = 1,\ B' = 0$ and (ii) $B = 0,\ B' = 1$. It is easy to show that $\exp(-i\Omega\tau_p)$ is an eigenvalue of M. For a given value of κ, Ω may be real or complex. Solutions with real Ω correspond to propagating states, while those with complex Ω represent evanescent states.

The real and imaginary parts of Ω are plotted in Figure 9 as a function of κ for $\tau_1 = 0.1$ (top) and $\tau_1 = 0.05$ (bottom). The combination $\kappa\tau_1^2/2$ was used because its value of 1 corresponds to the barrier height produced by each soliton. As seen in Figure 9, the real part of Ω vanishes in certain ranges of κ. These regions correspond to the momentum gaps of the grating. Several features are noteworthy in this figure. The number of momentum gaps depends on the value of τ_1 and increases as τ_1 is reduced. For larger values of κ, propagation bands become wider compared to the momentum gaps.

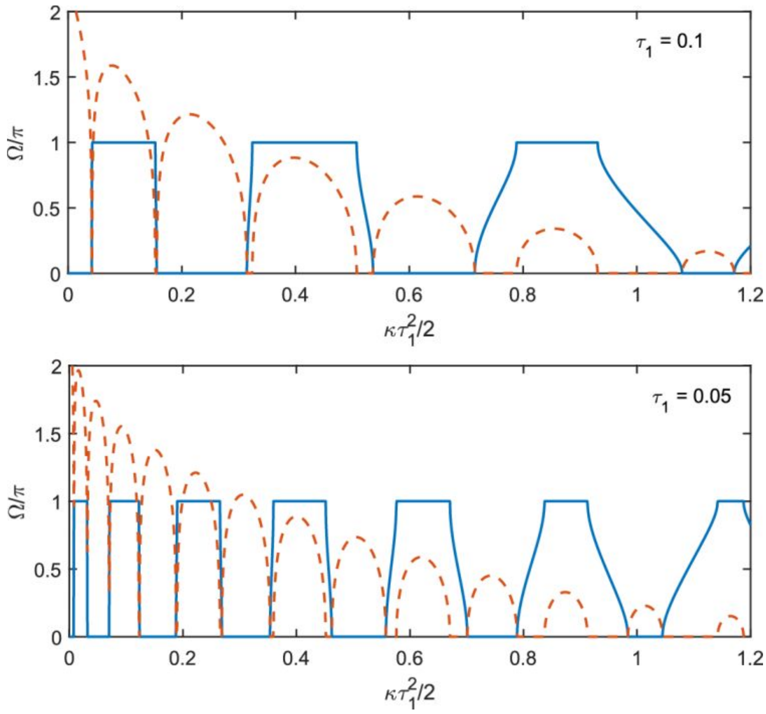

Figure 9. Band structure of a temporal grating for $\tau_1 = 0.1$ (**top**) and 0.05 (**bottom**). The real (solid line) and imaginary (dashed line) parts of Ω are plotted as a function of κ. Adapted with permission from [30] ©Optica Publishing Group.

Figure 10 shows the reflection of Gaussian pulse f when κ falls inside a momentum gap of the temporal grating [30]. The pulse is launched with the amplitude,

$$A(0,\tau) = \exp\left[-\frac{(\tau-\tau_s)^2}{2\tau_0^2} - i\Omega_i\tau\right], \quad (54)$$

using $\tau_0 = 10$, $\tau_s = -45$, and $\Omega_i = 7.63\pi$. The bottom panel displays spectral evolution of this pulse. The soliton train contained 21 pulses, spaced such that $\tau_1 = 0.1$, and was confined to the region $-10 < \tau < 10$, marked by two vertical dashed lines. As seen in Figure 10, probe pulse begins to interact with the grating at a distance $\xi = 1$ through the temporal interface located at $\tau = -10$. However, as $\kappa_i = \Omega_i^2/2$ falls in the momentum gap, the probe pulse is totally reflected by the STBG. It is mostly transmitted through when the κ value falls outside of a momentum gap.

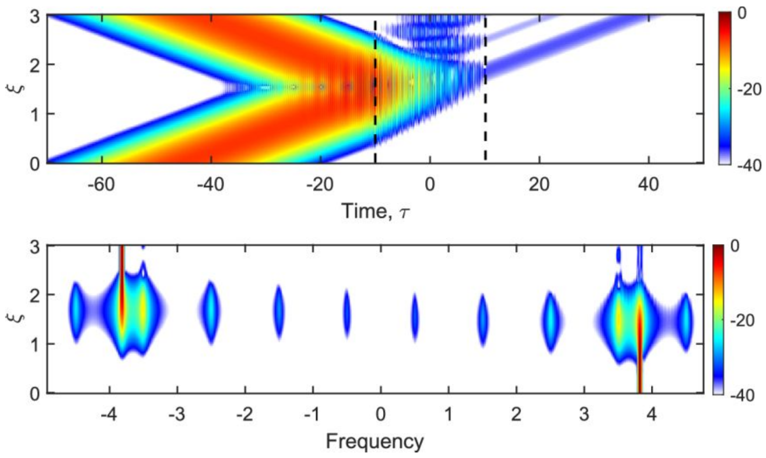

Figure 10. Total reflection of a probe pulse when κ falls inside a momentum gap of an STBG. Temporal (**top**) and spectral (**bottom**) evolution is shown along the fiber's length. Adapted with permission from [30] ©Optica Publishing Group.

6.2. Photonic Time Crystals

We briefly consider photonic time crystals (PTCs), devices where temporal index modulation occurs in a periodic fashion over their entire length on a single-cycle time scale [27–29]. The most striking feature of a PTC is the possibility of parametric amplification, possible because energy is not conserved in a thermodynamically open system. As we saw in Figure 9, PTCs exhibit momentum gaps, where the frequency of two eigenmodes flips from real to complex values. Using $\mathrm{Im}(\Omega) = \pm i\Gamma$ for the eigenvalues, the oscillatory part $e^{-i\Omega t}$ grows exponentially as $e^{\Gamma t}$ for one of these modes and results in its amplification. Energy for amplification comes from the source used for periodic temporal modulation of the refractive index. Figure 11 compares how the amplitude of a wave evolves in the spatial and temporal periodic systems. In the case of a spatial photonic crystal, optical power decays exponentially for any mode whose frequency falls in the energy gap of the crystal. In contrast, optical power can grow inside a photonic time crystal exhibiting momentum gaps.

The band structure of PTCs can be found using methods based on plane-wave expansion or transfer matrices [29]. The second method allows one to obtain the Floquet frequency ω_F in an analytic form for a PTC made of temporal slabs whose refractive index alternates between two values (n_1 and n_2) in a periodic fashion. An example of the band structure is shown in Figure 12, where the real and imaginary parts of Ω are plotted using $n_1 = 1$ and $n_2 = \sqrt{5}$. The modulation frequency ω_m is used to normalize both ω_F and the wave number k. The variable kc/ω_m, used along the x axis, corresponds to the wave's frequency relative to the modulation frequency ω_m. Similarly to Figure 9, the Floquet frequency becomes complex in each k gap, resulting in parametric amplification of the wave passing through such a PTC.

A general theory of such parametric amplification is complicated because multiple modes are excited inside the PTC at different frequencies when a single plane wave at a frequency ω_0 is launched into it. The problem is simplified considerably if only two dominant modes are considered. This approximation holds well when the frequency of incident wave satisfies the resonance condition $\omega_0 = \omega_m/2$. In this situation, the frequencies of the two counter-propagating coupled modes are $\omega_F \pm \omega_m/2$, and the underlying wave-mixing process is phase-matched. Further, the mode amplitudes A_1 and A_2 satisfy the coupled-mode equations [29]

$$\frac{dA_1}{dt} = i\eta A_2^*, \qquad \frac{dA_2}{dt} = i\eta A_1^*, \tag{55}$$

where losses have been ignored and the coupling parameter η depends on the contrast of periodic index modulation.

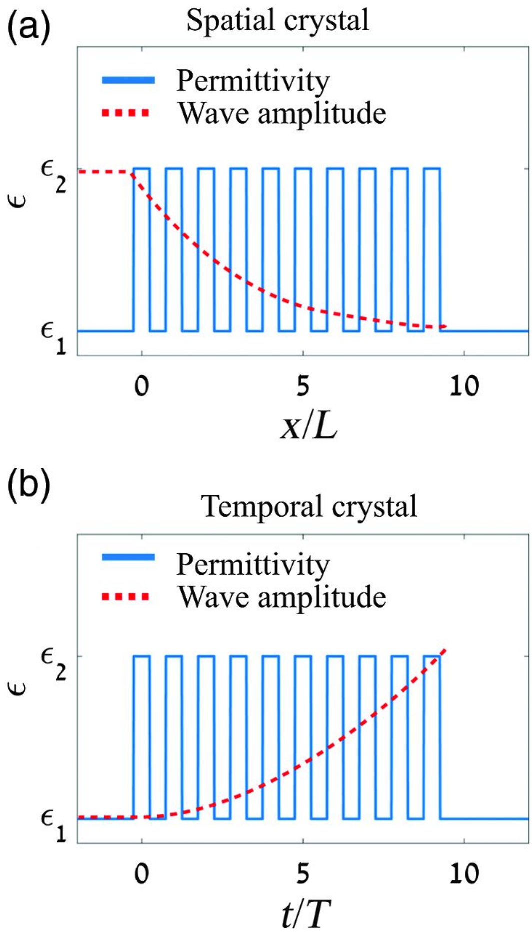

Figure 11. A schematic of (**a**) spatial and (**b**) temporal crystals exhibiting periodic variations in their dielectric constants. Dashed line shows that the amplitude of a wave grows inside a photonic time crystal. Adapted from [24] ©CC BY.

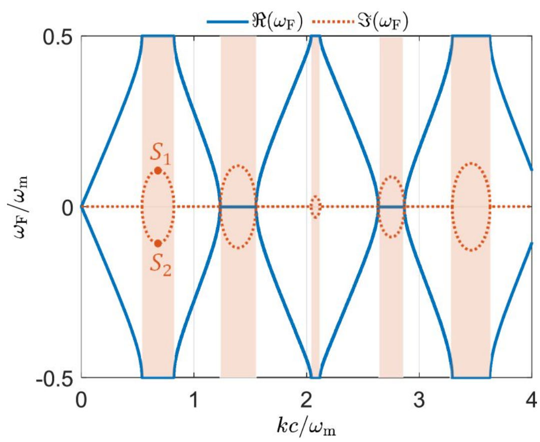

Figure 12. The band structure of a PTC formed using stepwise temporal modulation at a frequency ω_m. The real (solid line) and imaginary (dashed line) parts of ω_F are plotted as a function of kc/ω_m. The shaded regions show the momentum gaps. Adapted with permission from [29] ©Optica Publishing Group.

The preceding coupled-mode equations can be solved easily by noting that both A_1 and A_2 satisfy the same equation: $\frac{d^2 A_1}{dt^2} = |\eta|^2 A_1$. Using the initial conditions, $A_1(0) = A_0$ and $A_2(0) = 0$, the modal powers are found to grow exponentially with time as

$$|A_1((t)|^2 = A_0^2 \cosh^2(|\eta|t), \qquad |A_2((t)|^2 = A_0^2 \sinh^2(|\eta|t). \tag{56}$$

Thus, the input beam is amplified as it is transmitted through the PTC and its power increases by a factor of $\exp(2|\eta|t)/4$ after time such that $|\eta|t > 3$.

It is worth noting that two coupled equations similar to those in Equation (55) are also obtained for the nonlinear process of backward parametric amplification [45–47] in the undepleted-pump approximation. In this case, a signal beam with the amplitude A_1 is launched into a nonlinear crystal together with an intense pump beam. An idler beam propagating in the backward direction is generated through a three-wave mixing process when the phase-matching condition is satisfied. No pump beam is requited in the case of a PTC, and the idler is generated by the process that modulates its refractive index in a periodic fashion. Parametric amplification in this situation occurs only when the incident frequency is close to one half of the modulation frequency ($\omega_0 = \omega_m/2$).

7. Concluding Remarks

This review has focused on the concept of space–time duality in optics and its applications. Although this concept was originally based on the analogy between the diffraction of beams in space and the dispersion of pulses in time, it has been extended considerably in recent years. The first part of the review used time lenses and their applications as a simple example of the temporal analog of conventional lenses.

Novel phenomena emerge when optical pulses propagate through a nonlinear dispersive medium whose refractive index is modulated, both in space and time, in a traveling-wave fashion. Using optical fibers as an example of such a medium, we discussed the temporal analog of reflection at a moving index interface. A probe pulse incident at such an interface splits into two parts with different optical spectra such that the reflected part never crosses the interface. When the index change is large enough, the temporal analog of total internal reflection occurs, which allows one to construct time-domain waveguides that confine pulses to within a time window of fixed duration.

The use of nonlinear optics for creating moving index boundaries has allowed novel temporal analogs to be observed experimentally. The use of solitons through the Kerr effect indicates that such effects can be observed in silica fibers by employing a pump–probe configuration. A single solitons acts as a time-domain mirror that can be used to produce large spectral shifts through temporal reflection. Two closely spaced solitons can be used to make a temporal waveguide that confines probe pulses through multiple total internal reflections at both solitons. Two such solitons can also produce the temporal analog of a Fabry–Perot resonator by acting as partially reflecting mirrors.

An even more exotic temporal structure can be created by launching a periodic train of pump pulses that travel as fundamental solitons inside an optical fiber. Such a train of solitons induces periodic temporal modulations of the fiber's refractive index, leading to the formation of spatiotemporal Bragg gratings. Such a device exhibits the so-called momentum gaps that are temporal analogs of the frequency band gaps forming in spatially periodic gratings. A probe pulse is totally reflected from this type grating when the momentum of its photons lies inside of a momentum gap. A photonic analog of Anderson localization can also occur when some disorder is introduced into such periodic photonic time crystals.

It is important to stress that it was not possible to include all examples of space–time duality in this review because of space limitations. For example, spatial and temporal solitons are space–time duals, and this duality has been exploited in the context of Kerr frequency combs [12]. Some aspects of self-imaging in graded-index fibers [21] and the formation of multimode solitons in such fibers [48] are also related to space–time duality if we recall that spatial self-imaging is the dual of temporal oscillations of a harmonic oscillator.

Funding: This research was funded in part by U.S. National Science Foundation grant number ECCS-1933328.

Acknowledgments: The author is thankful to his collaborators, William Donaldson, Brent Plansinis, and Junchi Zhang, for working with him on the topics covered in this review.

Conflicts of Interest: The author declares no conflict of interest.

References

1. Tournois, P. Analogie optique de la compression d'impulsion. *CR Acad. Sci.* **1964**, *258*, 3839–3842.
2. Akhmanov, S.; Sukhorukov, A.; Chirkin, A. Nonstationary phenomena and space-time analogy in nonlinear optics. *Sov. Phys. JETP* **1969**, *28*, 748–757.
3. Kolner, B.H. Active pulse compression using an integrated electro-optic phase modulator. *Appl. Phys. Lett.* **1988**, *52*, 1122–1124.
4. Godil, A.; Auld, B.; Bloom, D. Time-lens producing 1.9 ps optical pulses. *Appl. Phys. Lett.* **1993**, *62*, 1047–1049.
5. Kolner, B.H. Space-time duality and the theory of temporal imaging. *IEEE J. Quantum Electron.* **1994**, *30*, 1951–1963.
6. Azaña, J.; Berger, N.K.; Levit, B.; Fischer, B. Spectro-temporal imaging of optical pulses with a single time lens. *IEEE Photon. Technol. Lett.* **2004**, *16*, 882–884.
7. van Howe, J.; Xu, C. Ultrafast Optical Signal Processing Based Upon Space-Time Dualities. *J. Lightwave Technol.* **2006**, *24*, 2649.
8. Torres-Company, V.; Lancis, J.; Andrés, P. *Space-Time Analogies in Optics*; Elsevier: Amsterdam, The Netherlands, 2011; Volume 56 , pp. 1–80. https://doi.org/https://doi.org/10.1016/B978-0-444-53886-4.00001-0.
9. Salem, R.; Foster, M.A.; Gaeta, A.L. Application of space-time duality to ultrahigh-speed optical signal processing. *Adv. Opt. Photon.* **2013**, *5*, 274–317. https://doi.org/10.1364/AOP.5.000274.
10. Agrawal, G.P. *Nonlinear Fiber Optics*, 6th ed.; Academic Press: Cambridge, MA, USA, 2019.
11. Kivshar, Y.S.; Agrawal, G.P. *Optical Solitons: From Fibers to Photonic Crystals*; Academic Press: Cambridge, MA, USA, 2003.
12. Lugiato, L.; Prati, F.; Gorodetsky, M.; Kippenberg, T. From the Lugiato–Lefever equation to microresonator-based soliton Kerr frequency combs. *Philos. Trans. R. Soc. A* **2018**, *376*, 20180113.
13. Mendonça, J.; Shukla, P. Time refraction and time reflection: Two basic concepts. *Phys. Scr.* **2002**, *65*, 160.
14. Xiao, Y.; Maywar, D.N.; Agrawal, G.P. Reflection and transmission of electromagnetic waves at a temporal boundary. *Opt. Lett.* **2014**, *39*, 574–577.
15. Plansinis, B.; Donaldson, W.; Agrawal, G. What is the temporal analog of reflection and refraction of optical beams? *Phys. Rev. Lett.* **2015**, *115*, 183901.
16. Biancalana, F.; Amann, A.; Uskov, A.V.; O'Reilly, E.P. Dynamics of light propagation in spatiotemporal dielectric structures. *Phys. Rev. E* **2007**, *75*, 046607. https://doi.org/10.1103/PhysRevE.75.046607.
17. Plansinis, B.W.; Donaldson, W.R.; Agrawal, G.P. Temporal waveguides for optical pulses. *J. Opt. Soc. Am. B* **2016**, *33*, 1112–1119.
18. Plansinis, B.W.; Donaldson, W.R.; Agrawal, G.P. Cross-phase-modulation-induced temporal reflection and waveguiding of optical pulses. *J. Opt. Soc. Am. B* **2018**, *35*, 436–445.
19. Zhang, J.; Donaldson, W.R.; Agrawal, G.P. Temporal reflection and refraction of optical pulses inside a dispersive medium: An analytic approach. *J. Opt. Soc. Am. B* **2021**, *38*, 997–1003.
20. Zhang, J.; Donaldson, W.R.; Agrawal, G.P. Impact of the boundary's sharpness on temporal reflection in dispersive media. *Opt. Lett.* **2021**, *46*, 4053–4056.
21. Agrawal, G.P. *Physics and Engineering of Graded-Index Media*; Cambridge University Press: Cambridge, UK, 2023.
22. Kashyap, R. *Fiber Bragg Gratings*, 2nd ed.; Academic Press: Cambridge, MA, USA, 2009.
23. Joannopoulos, J.D.; Johnson, S.G.; Winn, J.N.; Meade, R.D. *Photonic Crystals: Molding the Flow of Light*, 2nd ed.; Princeton University Press: Princeton, NJ, USA, 2009.
24. Galiffi, E.; Tirole, R.; Yin, S.; Li, H.; Vezzoli, S.; Huidobro, P.A.; Silveirinha, M.G.; Sapienza, R.; Alù, A.; Pendry, J.B. Photonics of time-varying media. *Adv. Photon.* **2022**, *4*, 014002.
25. Koutserimpas, T.T.; Monticone, F. Time-varying media, dispersion, and the principle of causality. *Opt. Mater. Express* **2024**, *14*, 1222–1236. https://doi.org/10.1364/OME.515957.
26. Zhang, J.; Donaldson, W.; Agrawal, G.P. Conservation law for electromagnetic fields in a space-time-varying medium and its implications. *Phys. Rev. A* **2024**, *110*, 043526. https://doi.org/10.1103/PhysRevA.110.043526.

27. Sharabi, Y.; Dikopoltsev, A.; Lustig, E.; Lumer, Y.; Segev, M. Spatiotemporal photonic crystals. *Optica* **2022**, *9*, 585–592.
28. Lustig, E.; Segal, O.; Saha, S.; Fruhling, C.; Shalaev, V.M.; Boltasseva, A.; Segev, M. Photonic time-crystals - fundamental concepts. *Opt. Express* **2023**, *31*, 9165–9170. https://doi.org/10.1364/OE.479367.
29. Asgari, M.M.; Garg, P.; Wang, X.; Mirmoosa, M.S.; Rockstuhl, C.; Asadchy, V. Theory and applications of photonic time crystals: A tutorial. *Adv. Opt. Photon.* **2024**, *16*, 958–1063. https://doi.org/10.1364/AOP.525163.
30. Zhang, J.; Donaldson, W.R.; Agrawal, G.P. Spatiotemporal Bragg gratings forming inside a nonlinear dispersive medium. *Opt. Lett.* **2024**, *49*, 5854–5857. https://doi.org/10.1364/OL.538147.
31. Born, M.; Wolf, E. *Principles of Optics*, 7th ed.; Cambridge University Press: Cambridge, UK, 1999.
32. Saleh, B.E.A.; Teich, M.C. *Fundamentals of Photonics*, 2nd ed.; Wiley: Hoboken, NJ, USA, 2012.
33. Agrawal, G.P. *Fiber-Optic Communication Systems*, 5th ed.; Wiley: Hoboken, NJ, USA, 2021.
34. Goda, K.; Jalali, B. Dispersive Fourier transformation for fast continuous single-shot measurements. *Nat. Photonics* **2013**, *7*, 102–112.
35. Godin, T.; Sader, L.; Khodadad Kashi, A.; Hanzard, P.H.; Hideur, A.; Moss, D.J.; Morandotti, R.; Genty, G.; Dudley, J.M.; Pasquazi, A.; et al. Recent advances on time-stretch dispersive Fourier transform and its applications. *Adv. Phys. X* **2022**, *7*, 2067487.
36. Chang, B.; Tan, T.; Du, J.; He, X.; Liang, Y.; Liu, Z.; Wang, C.; Xia, H.; Wu, Z.; Wang, J.; et al. Dispersive Fourier transform based dual-comb ranging. *Nat. Commun.* **2024**, *15*, 4990.
37. Bacot, V.; Labousse, M.; Eddi, A.; Fink, M.; Fort, E. Time reversal and holography with spacetime transformations. *Nat. Phys.* **2016**, *12*, 972–977.
38. Moussa, H.; Xu, G.; Yin, S.; Galiffi, E.; Ra'di, Y.; Alù, A. Observation of temporal reflection and broadband frequency translation at photonic time interfaces. *Nat. Phys.* **2023**, *19*, 863–868.
39. Ponomarenko, S.A.; Zhang, J.; Agrawal, G.P. Goos-Hänchen shift at a temporal boundary. *Phys/ Rev. A* **2022**, *106*, L061501. https://doi.org/10.1103/PhysRevA.106.L061501.
40. Tartara, L. Frequency shifting of femtosecond pulses by reflection at solitons. *IEEE J. Quantum Electron.* **2012**, *48*, 1439–1442. https://doi.org/10.1109/JQE.2012.2213584.
41. Okamoto, K. *Fundamentals of Optical Waveguides*, 3rd ed.; Academic Press: Cambridge, MA, USA, 2022.
42. Wang, S.F.; Mussot, A.; Conforti, M.; Zeng, X.L.; Kudlinski, A. Bouncing of a dispersive wave in a solitonic cage. *Opt. Lett.* **2015**, *40*, 3320–3323. https://doi.org/10.1364/OL.40.003320.
43. Zhang, J.; Donaldson, W.R.; Agrawal, G.P. Time-domain Fabry–Perot resonators formed inside a dispersive medium. *J. Opt. Soc. Am. B* **2021**, *38*, 2376–2382. https://doi.org/10.1364/JOSAB.428411.
44. Koufidis, S.F.; Koutserimpas, T.T.; McCall, M.W. Temporal analog of Bragg gratings. *Opt. Lett.* **2023**, *48*, 4500–4503.
45. Ding, Y.; Khurgin, J. Backward optical parametric oscillators and amplifiers. *IEEE J. Quantum Electron.* **1996**, *32*, 1574–1582.
46. Canalias, C.; Pasiskevicius, V. Mirrorless optical parametric oscillator. *Nat. Photonics* **2007**, *1*, 459–462.
47. Kasumova, R.J. Theory of a quasi-phase-matched optical parametric oscillator of a backward wave: Threshold and spectrum. *J. Opt. Soc. Am. B* **2024**, *41*, 1504–1512.
48. Sun, Y.; Parra-Rivas, P.; Agrawal, G.P.; Hansson, T.; Antonelli, C.; Mecozzi, A.; Mangini, F.; Wabnitz, S. Multimode solitons in optical fibers: A review. *Photonics Res.* **2024**, *12*, 2581–2632.